In-plane spin canting and 1/3-magnetization-plateaulike behavior in $S = 3/2$ Cr^{3+} kagome lattice antiferromagnets $Cs_2KCr_3F_{12}$ and $Cs_2NaCr_3F_{12}$

Masato Goto,[1,2,*] Hiroaki Ueda,[1] Chishiro Michioka,[1] Akira Matsuo,[3] Koichi Kindo,[3] Kento Sugawara,[4] Shintaro Kobayashi,[4] Naoyuki Katayama,[4] Hiroshi Sawa,[4] and Kazuyoshi Yoshimura[1,5,†]

[1]*Department of Chemistry, Graduate School of Science, Kyoto University, Kyoto 606-8502, Japan*

[2]*Institute for Chemical Research, Kyoto University, Kyoto 611-0011, Japan*

[3]*Institute for Solid State Physics, The University of Tokyo, Kashiwanoha, Kashiwa, Chiba 277-8581, Japan*

[4]*Department of Applied Physics, Graduate School of Engineering, Nagoya University, Aichi 464-8603, Japan*

[5]*Research Center for Low Temperature and Materials Sciences, Kyoto University, Kyoto 606-8502, Japan*

(Received 21 March 2018; published 20 June 2018)

We have investigated the structural and magnetic properties of $S = 3/2$ Cr^{3+} Heisenberg-like kagome lattice antiferromagnets $Cs_2KCr_3F_{12}$ and $Cs_2NaCr_3F_{12}$ using single crystals. Each compound has a slightly distorted kagome lattice, although the space groups differ for the two compounds. The magnetic data suggest that each compound exhibits the formation of antiferromagnetic ordering with in-plane-spin canting approximately below 6 K. The in-plane coplanar structures are clearly different from disordered ground states of the isostructural Ti^{3+} compounds and out-of-plane coplanar structures of the V^{3+} compounds, which is mainly caused by the differences in the strength of quantum fluctuation and the strength of magnetic anisotropy for these three spin systems. In contrast, as well as the Ti^{3+} and V^{3+} compounds, the magnetization curves show 1/3-magnetization-plateaulike anomalies.

DOI: 10.1103/PhysRevB.97.224421

I. INTRODUCTION

Geometrically frustrated antiferromagnets often cause unconventional magnetic phenomena originating in the suppression of Néel ordering [1,2]. In particular, kagome lattice antiferromagnets (KLAFs) have attracted much attention from the viewpoint of the interplay between quantum fluctuation and spin frustration, which may induce exotic disordered ground states [3–16] and magnetic-field-induced phases [17–19]. Interestingly, the ground states are considered to depend strongly on quantum spin numbers S. For example, one expects a gapped [3–8] or gapless [9–12] spin liquid ground state in $S = 1/2$ KLAFs, and a hexagonal [13,14] or trigonal [15,16] valence bond solid state was predicted in $S = 1$ KLAFs. In the classical limit, the macroscopic degeneracy of 120° coplanar structures is expected due to chiral degrees of freedom (clockwise or counterclockwise spin arrangement) in each triangle. In contrast, under high magnetic fields, a 1/3-magnetization plateau has been proposed to appear at least in the range of $S = 1/2$–2 [17–19].

To understand the effects of quantum fluctuation on the magnetic properties of KLAFs, experimentally comparative studies of several compounds are essential in addition to theoretical studies. However, such experimental studies are difficult, since all compounds have some discrepancies from the ideal system, such as the lattice distortion of a kagome lattice, next-nearest-neighbor interactions, interlayer interactions, the disorder of constituent ions, and the Dzyaloshinsky-Moriya (DM) interaction. These discrepancies depend mainly on the crystal structure and strongly affect the magnetic properties of KLAFs [20–24]. For example, next-nearest-neighbor interactions and the DM interaction stabilize the $\sqrt{3} \times \sqrt{3}$ [20] type 120° structure and $q = 0$ [21,22] type 120° structures, respectively. Experimentally, although some KLAFs [25–42], such as $S = 1/2$ herbertsmithite $ZnCu_3(OH)_6Cl_2$ [25–29], vesignieite $BaCu_3V_2O_8(OH)_2$ [30–32], and $S = 3/2$ jarosite $KCr_3(OH)_6(SO_4)$ [33,34], have been studied intensively, their different crystal structures make it hard to compare their magnetic properties in terms of quantum fluctuation. Thus, it is necessary to explore KLAFs that have similar crystal structures and a variety of S.

Previously, we reported the crystal structures and magnetic properties of three $S = 1/2$ Ti^{3+} kagome fluorides $Cs_2KTi_3F_{12}$, $Cs_2NaTi_3F_{12}$, and $Rb_2NaTi_3F_{12}$ [43] and three $S = 1$ $Cs_2KV_3F_{12}$, $Cs_2NaV_3F_{12}$, and $Rb_2NaV_3F_{12}$ [44]. Subsequently, we have discovered two Cr^{3+} kagome fluorides $Cs_2KCr_3F_{12}$ and $Cs_2NaCr_3F_{12}$. The presence of these two $S = 3/2$ Cr^{3+} compounds with isostructural KLAFs $A_2BM_3F_{12}$ (A = Cs,Rb; B = K,Na; M^{3+} = Ti^{3+},V^{3+}) enables us to study the effects of the interplay between spin frustration and quantum fluctuation in the case of $S = 1/2$–3/2, which is very novel in real kagome systems.

In this paper, we report the crystal structures and magnetic properties of two $S = 3/2$ Heisenberg-like KLAFs $Cs_2BCr_3F_{12}$ (B = K,Na). Each compound has a slightly distorted kagome lattice, while the crystal structure at room temperature differs between two compounds. In addition, $Cs_2KCr_3F_{12}$ exhibits a structural transition at approximately 270 K. An antiferromagnetic phase transition is observed in both compounds at approximately 6 K, whereas only

*goto.masato.8s@kyoto-u.ac.jp
†kyhv@kuchem.kyoto-u.ac.jp

$Cs_2KCr_3F_{12}$ shows spontaneous magnetization below the transition temperature. These high-field magnetization curves show 1/3-magnetization-plateaulike behavior at 17–22 T irrespective of the direction of a magnetic field. We discuss the magnetic properties, taking into account those of other kagome systems and $S = 1/2$ $A_2BTi_3F_{12}$ and $S = 1$ $A_2BV_3F_{12}$.

II. EXPERIMENT

Single crystals of $Cs_2BCr_3F_{12}$ (B = K,Na) were grown using flux methods in Ni crucibles under an Ar atmosphere. Dried alkali-metal fluorides CsF and BF and purified CrF_3 were used as the starting materials. Mixtures of alkali-metal chlorides were used as fluxes.

X-ray diffraction data of obtained crystals were collected using the BL8A beamline with a wavelength of 0.6890 Å ($Cs_2NaCr_3F_{12}$ for structural analyses and $Cs_2BCr_3F_{12}$ for the temperature dependence of lattice constants) at the Photon Factory, KEK, Japan, and using the BL02B1 beamline [45] with a wavelength of 0.4965 Å ($Cs_2KCr_3F_{12}$ for structural analyses) at SPring-8, Japan. We used crystals with a typical size of $70 \times 50 \times 20$ μm^3. The samples were cooled by a nitrogen-gas-flow-type refrigerator. In $Cs_2BCr_3F_{12}$, there exist preformed domains: non-merohedral twinning for $Cs_2KCr_3F_{12}$ in the high-temperature (HT) phase and $Cs_2NaCr_3F_{12}$ or merohedral twinning for $Cs_2KCr_3F_{12}$ in the low-temperature (LT) phase. The data reduction by the detwinning of non-merohedral domains was performed using software developed in-house [46], whereas that by the detwinning of merohedral domains was performed using the SHELXL-97 software [47]. The structural parameters including anisotropic displacement parameters were refined using a full-matrix least-squares method with the SHELXL-97 software [47]. The detailed conditions for structural analyses are listed in Table I.

dc magnetization measurements were performed in a temperature range of 2–300 K using a superconducting quantum interference device magnetometer (Quantum Design MPMS-XL system) in the Research Center for Low Temperature and Materials Sciences, Kyoto University. Magnetization curves up to approximately 60 T were measured using an induction method with a multilayer pulsed magnet at the International MegaGauss Science Laboratory of the Institute for Solid State Physics at the University of Tokyo.

TABLE I. Experimental details and crystallographic data of $Cs_2BCr_3F_{12}$. The numbers in parentheses are the standard deviations in the last significant figures.

	$Cs_2NaCr_3F_{12}$	$Cs_2KCr_3F_{12}$	
	125 K	320 K	120 K
Wavelength (Å)	0.6890	0.4965	0.4965
Space group	$P2_1/m$	$C2/n$	$P3_121$
a (Å)	12.566(3)	12.704(4)	7.3260(16)
b (Å)	7.2837(10)	7.338(3)	7.3260(16)
c (Å)	7.401(2)	15.234(8)	18.719(7)
β (deg)	125.019(10)	124.33(3)	
Z	2	4	3
d (Å)	0.4-6.1	0.5-6.3	0.4-6.4
Completeness (%)	89.2	93.4	97.1
$N_{\text{total,obs}}$	25476	26388	54252
$N_{\text{uniq,obs}}$	6018	3628	6556
$N_{\text{uniq}}[F_o > 4\sigma(F_o)]$	4693	2950	5698
$R_1[F_o > 4\sigma(F_o)]$	0.0222	0.0303	0.0294
$\omega R_2(F_o^2)$	0.0397	0.0759	0.0644

TABLE II. The atomic coordinates and equivalent isotropic displacement parameters of $Cs_2NaCr_3F_{12}$ at 125 K. The numbers in parentheses are the standard deviations in the last significant figures.

Atom	x	y	z	U_{eq} (Å^2)
Cs1	0.617905(6)	3/4	0.627706(11)	0.01061(2)
Cs2	0.136514(6)	1/4	0.617103(10)	0.00955(2)
Na1	0.74569(4)	1/4	0.52648(6)	0.00638(6)
Cr1	0	0	0	0.00336(2)
Cr2	1/2	0	0	0.00321(2)
Cr3	0.769980(13)	1/4	0.056103(19)	0.00319(2)
F1	0.01432(5)	1/4	0.93527(9)	0.00792(8)
F2	0.58025(4)	0.45554(6)	0.29937(6)	0.00902(7)
F3	0.10944(4)	0.93635(6)	0.90438(7)	0.00782(6)
F4	0.14605(4)	0.02441(6)	0.28996(6)	0.00845(6)
F5	0.55836(5)	3/4	0.07139(9)	0.00733(8)
F6	0.34064(4)	0.55528(6)	0.96875(7)	0.00813(6)
F7	0.14809(6)	3/4	0.63833(9)	0.00946(11)
F8	0.31873(5)	3/4	0.24835(9)	0.00937(9)

III. RESULTS

A. Crystal structure

In our systematic studies of fluorides, we discovered two $S = 3/2$ kagome fluorides $Cs_2NaCr_3F_{12}$ and $Cs_2KCr_3F_{12}$ in addition to the previously reported three $S = 1/2$ Ti^{3+} fluorides $A_2BTi_3F_{12}$ [43] and three $S = 1$ $A_2BV_3F_{12}$ [44]. We succeeded in growing hexagonal-shaped crystals of $Cs_2BCr_3F_{12}$ with a typical size of $1.8 \times 1.8 \times 0.7$ mm^3. The crystals are yellowish green, indicating that they are insulators. In $Cs_2BCr_3F_{12}$, the crystals consist of some domains, as revealed by x-ray diffraction and polarizing microscope measurements. The domains are thought to be formed when a HT trigonal structure becomes a monoclinic structure during the cooling process of the crystal growth. The b axis of each domain is parallel to one of the Cr-Cr chains in the kagome plane. Table I shows structural parameters of $Cs_2BCr_3F_{12}$. For $Cs_2KCr_3F_{12}$, the parameters at both 320 and 120 K are listed, since the crystal structure at 120 K (in the LT phase) is different from that at room temperature (in the HT phase). The atomic coordinates and equivalent isotropic displacements of $Cs_2NaCr_3F_{12}$ at 125 K, $Cs_2KCr_3F_{12}$ at 320 K, and $Cs_2KCr_3F_{12}$ at 120 K are collected in Tables II, III, and IV, respectively. While $Cs_2NaCr_3F_{12}$ crystallizes in a monoclinic system of $P2_1/m$, $Cs_2KCr_3F_{12}$ in the HT phase crystallizes in a monoclinic system of $C2/n$ with an $a \times b \times 2c$ unit cell compared with that of $Cs_2NaCr_3F_{12}$ [Figs. 1(a) and 1(b)]. In addition, as shown in Fig. 2, $Cs_2KCr_3F_{12}$ shows a structural transition at $T_S \sim 270$ K, and the crystal structure changes to a trigonal system of $P3_121$ [Fig. 1(c)]. At T_S, $Cs_2KCr_3F_{12}$ exhibits

TABLE III. The atomic coordinates and equivalent isotropic displacement parameters of $Cs_2KCr_3F_{12}$ at 320 K. The numbers in parentheses are standard deviations in the last significant figures.

Atom	x	y	z	U_{eq} (Å^2)
Cs1	0.63236(15)	0.72219(2)	0.320433(11)	0.02849(5)
K1	3/4	0.23060(7)	1/4	0.01869(9)
Cr1	0	0	0	0.00849(6)
Cr2	1/2	0	0	0.00875(6)
Cr3	3/4	1/4	0	0.00939(6)
F1	0.03109(14)	0.24973(14)	0.48301(13)	0.0248(3)
F2	0.61730(11)	0.51857(19)	0.14538(9)	0.0300(3)
F3	0.13486(11)	0.93779(15)	0.98357(11)	0.0239(2)
F4	0.08134(12)	0.0294(2)	0.64563(9)	0.0283(3)
F5	0.14646(13)	0.7051(2)	0.85452(10)	0.0253(3)
F6	0.33772(10)	0.93532(15)	0.97414(10)	0.0197(2)

sudden decreases of lattice parameters c' and β and the relative sliding distance between the kagome planes δ/a, where c', β, δ, and a are shown in the inset of Fig. 2. An effect of the structural change on the magnetic property is discussed later.

Although $Cs_2KCr_3F_{12}$ and $Cs_2NaCr_3F_{12}$ have different space groups, all the crystal structures of $Cs_2BCr_3F_{12}$ can be understood as an ordered structure of the cubic modified pyrochlore $A'B'_2X_6$, which includes $Rb(Ni_{0.5}Cr_{0.5})_2F_6$ [48]. In $Cs_2BCr_3F_{12}$, Cr kagome layers and B triangular layers are alternately stacked in the pyrochlore of the B' site. Thus, the magnetic Cr^{3+} kagome layers are well separated by layers of the nonmagnetic large alkali-metal ions of Cs^+ and B^+. The interlayer superexchange couplings Cr-F-Cs(B)-F-Cr are much weaker than the in-plane couplings Cr-F-Cr, which produce a quasi-2D kagome lattice.

As shown in Fig. 1, the small distortion of each kagome lattice produces several Cr^{3+} sites and several types of in-plane exchange interactions J_i ($i = 1,2,\ldots$), the number of which depends on the space group. For $Cs_2NaCr_3F_{12}$, both Cr1 and Cr2 form one-dimensional chains along the b axis, and the chains of Cr1 and Cr2 are bridged by Cr3. The most remarkable difference between the crystal structures of $Cs_2NaCr_3F_{12}$ and $Cs_2KCr_3F_{12}$ is the difference between the undulations of kagome lattices. The amplitude of the undulation is roughly

TABLE IV. The atomic coordinates and equivalent isotropic displacement parameters of $Cs_2KCr_3F_{12}$ at 120 K. The numbers in parentheses are the standard deviations in the last significant figures.

Atom	x	y	z	U_{eq} (Å^2)
Cs1	0.632819(17)	0.959684(16)	0.953139(5)	0.00981(2)
K1	0.30720(6)	0.3072(6)	0	0.00727(5)
Cr1	0.65433(4)	0.49995(4)	0.832492(15)	0.00368(3)
Cr2	0.15521(5)	0	5/6	0.00369(4)
F1	0.86341(17)	0.41886(15)	0.84869(6)	0.00869(14)
F2	0.65188(17)	0.4478(2)	0.73475(6)	0.00886(17)
F3	0.86361(17)	0.79194(17)	0.81595(6)	0.00847(15)
F4	0.1287(2)	0.94563(16)	0.93097(5)	0.01037(16)
F5	0.44666(16)	0.20827(17)	0.84951(6)	0.00844(15)
F6	0.65439(19)	0.5518(2)	0.92947(6)	0.00968(17)

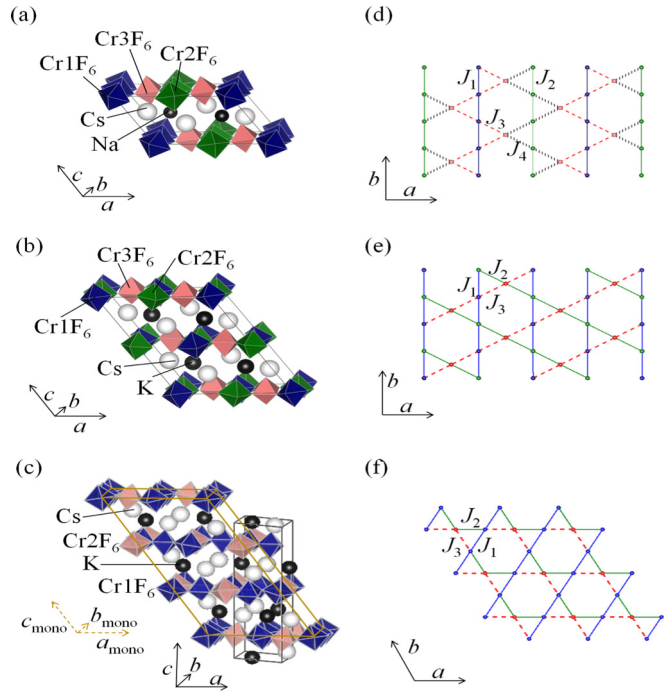

FIG. 1. The crystal structures of (a) $Cs_2NaCr_3F_{12}$ (monoclinic, $P2_1/m$), (b) $Cs_2KCr_3F_{12}$ in the high-temperature (HT) phase (monoclinic, $C2/n$), and (c) $Cs_2KCr_3F_{12}$ in the low-temperature (LT) phase (trigonal, $P3_121$). The yellow lines in (c) indicate the corresponding monoclinic cell. The exchange network in the kagome layer for (d) $Cs_2NaCr_3F_{12}$, (e) $Cs_2KCr_3F_{12}$ in the HT phase, and (f) $Cs_2KCr_3F_{12}$ in the LT phase.

evaluated by a value $c(z^{Cr}_{max} - z^{Cr}_{min})\sin\beta$, where z^{Cr}_{max} and z^{Cr}_{min} are the maximum and minimum of the atomic coordinates z among the Cr sites of each kagome layer, respectively. While the small undulation for $Cs_2NaCr_3F_{12}$ (0.34 Å) is present, the undulation for $Cs_2KCr_3F_{12}$ is absent (HT phase) or negligibly small (0.01 Å: LT phase). As a result, Cr1 and Cr2 chains are inequivalent for $Cs_2NaCr_3F_{12}$ due to the absence of the inversion symmetry of Cr3, whereas all chains along the b axis are equivalent for $Cs_2KCr_3F_{12}$ in the HT phase. In $A_2BM_3F_{12}$ (M = Ti,V,Cr), the undulation becomes small with increasing ionic radii of the constituent alkali metals r_{A^+} and r_{B^+}, and with decreasing $r_{M^{3+}}$ [43,44]. With decreasing r_{A^+} and r_{B^+}, the space around the alkali-metal ions becomes large, and all B^+ ions slightly shift above or below the midpoint between kagome planes (see z of Na for $Cs_2NaCr_3F_{12}$). In concert with the undulation of B^+, some M^{3+} ions slightly shift above and other ones shift below the kagome plane, which produces an undulation of the kagome lattice. That is why the undulation for $Cs_2KCr_3F_{12}$ with large K^+ is absent in the HT phase and very small in the LT phase.

Although the undulation is negligible in $Cs_2KCr_3F_{12}$, the HT phase has two Cr^{3+} sites in each chain along the b axis, which is different from the structure of $Cs_2NaCr_3F_{12}$. Moreover, the crystal structure changes to a trigonal system at T_S. Below T_S, $Cs_2KCr_3F_{12}$ has two Cr sites and three J_i, as shown in Figs. 1(c) and 1(f). In $A_2BM_3F_{12}$ (M = Ti,V,Cr), while all $Cs_2NaM_3F_{12}$ and $Rb_2NaM_3F_{12}$ crystallize in the monoclinic system of $P2_1/m$, $Cs_2KV_3F_{12}$ has the space group

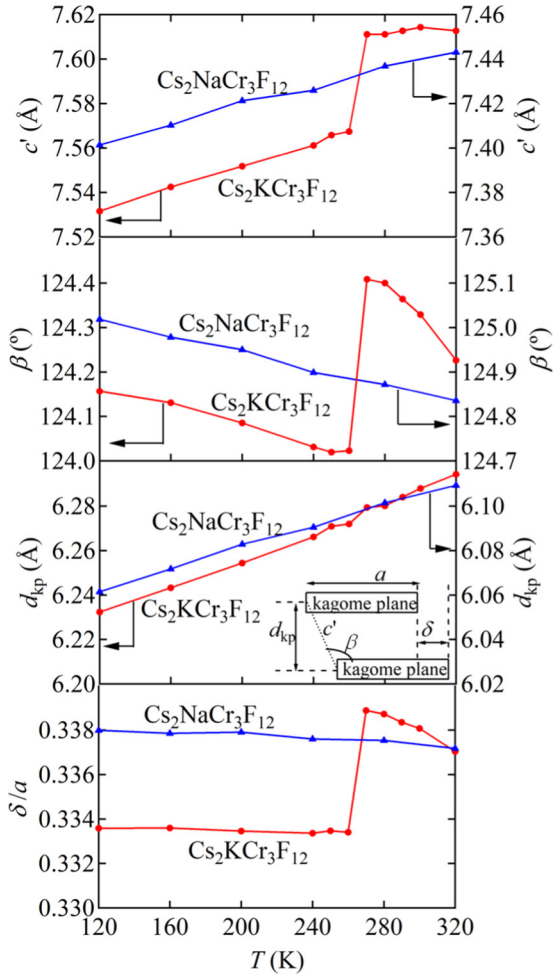

FIG. 2. The temperature dependence of lattice parameters c' and β, the distance between the nearest-neighbor kagome planes d_{kp}, and the relative sliding distance between the nearest-neighbor kagome planes δ/a, where $d_{kp} = c' \sin\beta$ and $\delta = -c' \cos\beta$ as shown in a schematic chart in the inset.

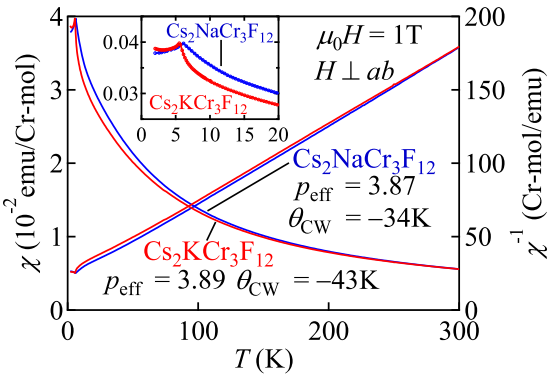

FIG. 3. The temperature dependence of the magnetic susceptibility $\chi = M/H$ and their inverses χ^{-1} of $Cs_2BCr_3F_{12}$ under $\mu_0 H = 1$ T for $H \perp ab$. The inset shows enlarged χ-T curves around anomalies. All the measurements were performed under field-cooling conditions.

of $P2_1/c$ with two V^{3+} sites in each chain. Thus, only the system $Cs_2KM_3F_{12}$ with a negligibly small undulation shows the clear M^{3+} dependence of crystal structures. The result would be understood as follows. In the case of a relatively large undulation (when lattice instability is dominant), the space group tends to be fixed to $P2_1/m$. In contrast, when the undulation is very small, various crystal structures can exist due to the interplay between the small lattice instability and degrees of freedom of M^{3+}, although the detail is unclear.

Upon decreasing the undulation, differences among the ∠Cr-F-Cr values and among the Cr-Cr distances in the nearest-neighbor Cr ions, which induce differences among several J_i, become small. The ∠Cr-F-Cr values are within the range of 141.0°–144.5° for $Cs_2NaCr_3F_{12}$, 143.5°–145.4° for $Cs_2KCr_3F_{12}$ in the HT phase, and 142.9°–144.3° for $Cs_2KCr_3F_{12}$ in the LT phase. The difference between the largest and smallest Cr-Cr distances is 0.6% for $Cs_2NaCr_3F_{12}$, 0.1% for $Cs_2KCr_3F_{12}$ in the HT phase, and 0.2% for the LT phase. The small differences among the ∠Cr-F-Cr values and among the Cr-Cr distances suggest that all J_i at least have the same sign in $Cs_2BCr_3F_{12}$. In particular, the distortion of the kagome lattice of $Cs_2KCr_3F_{12}$ is as small as that of $BaCu_3V_2O_8(OH)_2$ with a nearly undistorted kagome lattice (Cu-Cu: 0.07–0.2%) [31]. Thus, $Cs_2KCr_3F_{12}$ is expected to have nearly isotropic J_i, while $Cs_2NaCr_3F_{12}$ has rather anisotropic J_i.

B. Magnetic properties at low magnetic fields

Figure 3 shows the temperature T dependence of the magnetic susceptibility $\chi = M/H$ and its inverse χ^{-1} under $\mu_0 H = 1$ T for $H \perp ab$, where M is the magnetization, H is a magnetic field, and ab corresponds to the kagome plane. At high temperatures, both χ-T curves show the Curie-Weiss-like behavior, and thus χ^{-1}-T curves are almost linear. For $Cs_2KCr_3F_{12}$, no anomaly is observed at $T_s \sim 270$ K in χ-T, which suggests a small change of J_i at T_s. The effective Bohr magneton number p_{eff} and the Weiss temperature θ_{CW}, which are shown in Fig. 3, are obtained from the Curie-Weiss fittings $\chi = C/(T - \theta_{CW})$ between 100 and 300 K. The obtained p_{eff} values are in good agreement with the theoretical value 3.87 for $S = 3/2$ and $g = 2$. Negative θ_{CW} values indicate dominant antiferromagnetic interactions in $Cs_2BCr_3F_{12}$, which suggests that all nearest-neighbor J_i are antiferromagnetic.

With decreasing T, χ-T shows a kink at $T_N = 5.5$ K for $Cs_2KCr_3F_{12}$ and at 6.1 K for $Cs_2NaCr_3F_{12}$ (see the inset of Fig. 3), which indicates the formation of magnetic ordering. Frustration indices $|\theta_{CW}|/T_N$ are obtained to be 7.8 for $Cs_2KCr_3F_{12}$ and 5.5 for $Cs_2NaCr_3F_{12}$. The large $|\theta_{CW}|/T_N$ values suggest strong spin frustration effects in $Cs_2BCr_3F_{12}$.

To examine the magnetic states below T_N in detail, we measured M/H-T curves under several H for $H \perp ab$ and $H \parallel ab$, which are shown in Fig. 4. For $H \perp ab$, the M/H-T curves of both compounds are nearly independent of $\mu_0 H$, and each M/H-T shows a peak near T_N. In contrast, for $H \parallel ab$, the M/H-T curves below T_N depend strongly on $\mu_0 H$. In addition, M/H-T under 0.1 T for $Cs_2KCr_3F_{12}$ is clearly different from that for $Cs_2NaCr_3F_{12}$. For $Cs_2KCr_3F_{12}$, M/H under 0.1 T increases rapidly near T_N and approaches a constant value with decreasing T (see the inset of Fig. 4). With decreasing $\mu_0 H$,

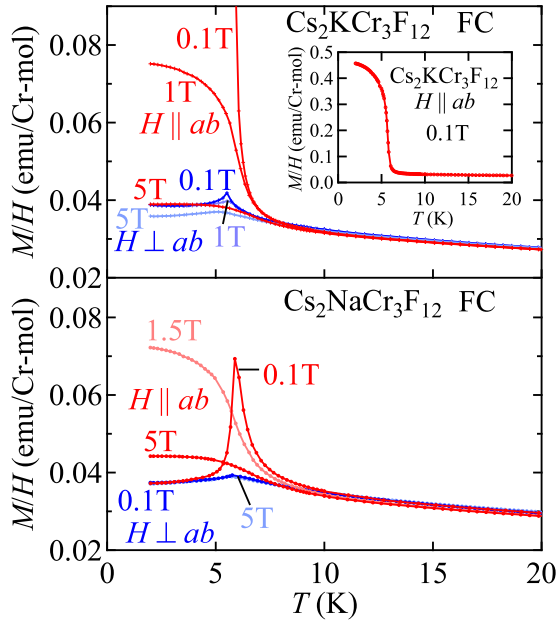

FIG. 4. The temperature dependence of M/H under several H for $H \perp ab$ and $H \parallel ab$. The inset shows M/H-T of $Cs_2KCr_3F_{12}$ under 0.1 T for $H \parallel ab$. All the measurements were performed under field-cooling conditions.

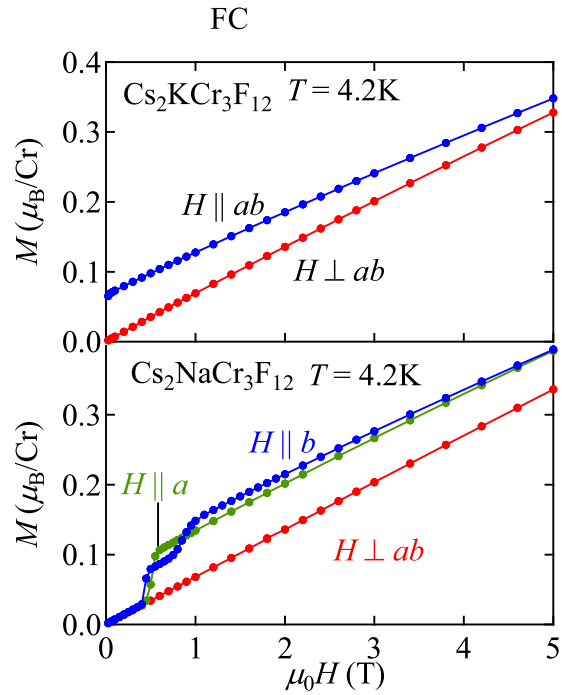

FIG. 5. The M-H curves up to 5 T at 4.2 K, where $H \parallel a$ and $H \parallel b$ denote the direction of H for one of the crystal domains. For $Cs_2KCr_3F_{12}$, M-H for $H \parallel b$ is plotted as that for $H \parallel ab$, since negligible in-plane magnetic anisotropy is observed. All the measurements were performed under field-cooling conditions.

each M/H increases at the same T, which corresponds to weak ferromagnetic behavior. For $Cs_2NaCr_3F_{12}$, M/H-T under 0.1 T shows a sharp peak near T_N, although the M/H-T curves under higher $\mu_0 H$ are similar to those of $Cs_2KCr_3F_{12}$.

In addition to the M/H-T data, the M-H curves help us to clarify the magnetic states below T_N, which are shown in Fig. 5. For $H \perp ab$, M of both compounds increases almost linearly with increasing $\mu_0 H$, which is consistent with the M/H-T data. For $H \parallel ab$, M-H of $Cs_2KCr_3F_{12}$ shows spontaneous magnetization with $M_{sp} \sim 0.08\mu_B$/Cr, which suggests the presence of canted spin moments in the kagome plane. In contrast, for $Cs_2NaCr_3F_{12}$, M-H for $H \parallel ab$ shows no M_{sp}, and in-plane magnetic anisotropy is observed. For $H \parallel a$ (see the caption of Fig. 5), M jumps at 0.5 T and then increases roughly linearly with increasing $\mu_0 H$, whereas M for $H \parallel b$ jumps at 0.4 and 0.8 T successively, then increases roughly linearly, and almost coincides with M for $H \parallel a$ above 2 T. By extrapolating linearly from the high $\mu_0 H$ range into 0 T, we obtain approximately $0.08\mu_B$/Cr for $H \parallel a$ and $0.10\mu_B$/Cr for $H \parallel b$, which are almost the same as M_{sp} of $Cs_2KCr_3F_{12}$. The spin-flip-like jumps of M for $H \parallel a$ and $H \parallel b$ suggest that in-plane spin canting occurs in each kagome layer of $Cs_2NaCr_3F_{12}$ and that the canted moments are canceled out among the layers in the ground state. The successive jumps of M for $H \parallel b$ are considered to be due to the presence of domains, although the detail is unknown.

C. High-field magnetization

From the M/H-T and M-H data, $Cs_2NaCr_3F_{12}$ and $Cs_2KCr_3F_{12}$ are revealed to form magnetic ordering below approximately 6 K. In the isostructural KLAFs $S = 1/2$ $A_2BTi_3F_{12}$ [43] and $S = 1$ $A_2BV_3F_{12}$ [44], interesting magnetic-field-induced phases, including magnetization plateaus, are observed at low temperatures. To examine the effects of S under high magnetic fields, we measured M-H curves up to 60 T for $H \perp ab$ and $H \parallel ab$ at 1.3 and 4.2 K for $Cs_2KCr_3F_{12}$ and $Cs_2NaCr_3F_{12}$, which are shown in Fig. 6. For $Cs_2KCr_3F_{12}$, dM/dH at 1.3 K for both H directions decreases gradually with increasing $\mu_0 H$ from 0 T, shows a broad minimum at approximately 19 T, and begins to increase above 19 T. Correspondingly, as indicated by arrows, an inflection point is observed in each M-H at approximately 1/3 of the full moment, which is considered to be a sign of the 1/3-magnetization plateau. At 4.2 K, dM/dH for both H directions shows a more distinct dip at approximately 1/3 of the full moment, which suggests the stabilization of the 1/3-magnetization plateau state due to thermal energy. A similar behavior is also observed in $Cs_2NaCr_3F_{12}$ at approximately 18 T. Among $S = 3/2$ KLAFs, jarosite $KCr_3(OH)_6(SO_4)_2$ was reported to exhibit a similar 1/3-magnetization-plateaulike anomaly only under in-plane fields [33].

Above the inflection points, anisotropy is clearly observed in M-H of both compounds at only 1.3 K. For $Cs_2KCr_3F_{12}$, while M-H at 1.3 K for $H \perp ab$ shows no anomaly above 19 T and shows saturation at 50 T, that for $H \parallel ab$ increases rapidly at 40 T. The anomaly is more distinct in dM/dH-H, which is observed as a sharp peak at 40 T. A spin rearrangement is considered to occur at 40 T probably due to the small easy-plane anisotropy and chiral degrees of freedom in the kagome lattice. A small peak of dM/dH-H is also observed in $Cs_2NaCr_3F_{12}$ at 38 T and at 1.3 K only for $H \parallel ab$, which may correspond to the anomaly in $Cs_2KCr_3F_{12}$ at 40 T.

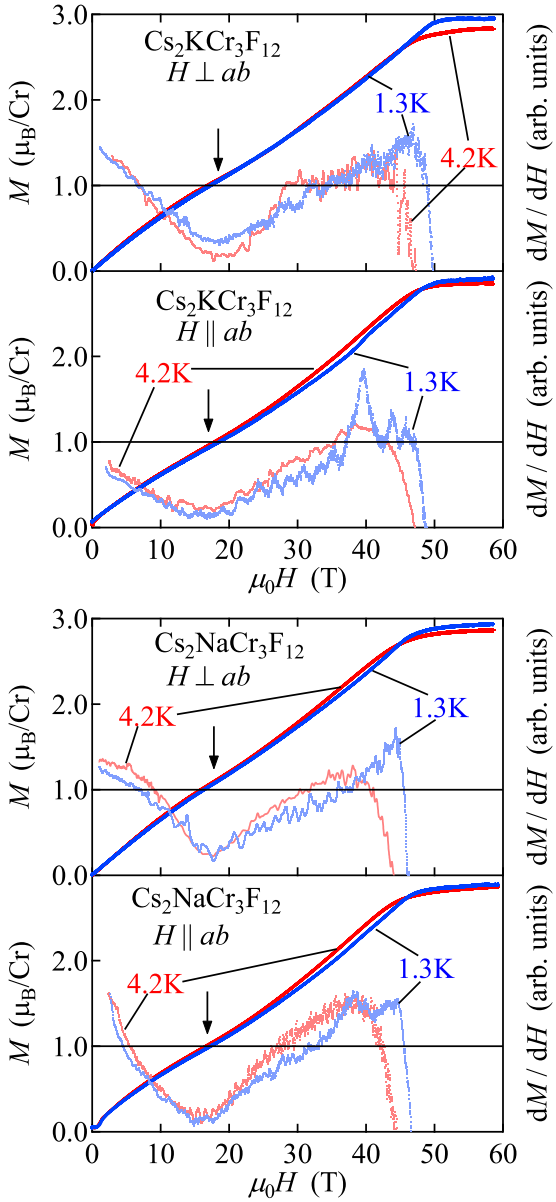

FIG. 6. The magnetization curves M-H and the differential magnetization curves dM/dH-H up to approximately 60 T in $Cs_2BCr_3F_{12}$ at 1.3 and 4.2 K for $H \perp ab$ and $H \parallel ab$. The horizontal lines indicate $M = 1/3M_{sat}$, where $M_{sat} = 3\mu_B$ is the saturation magnetization. Arrows indicate inflection points of the M-H curves.

IV. DISCUSSION

Summarizing our experimental results, two $S = 3/2$ Heisenberg-like KLAFs $Cs_2BCr_3F_{12}$ (B = K,Na) have dominant in-plane antiferromagnetic interactions with $\theta_{CW} \sim -40$ K and exhibit magnetic ordering with in-plane spin canting, while only $Cs_2KCr_3F_{12}$ shows M_{sp} for $H \parallel ab$. In addition, both compounds show 1/3-magnetization-plateaulike anomalies irrespective of the direction of H. We discuss the detailed magnetic properties, taking into account those of other kagome systems and isostructural $A_2BTi_3F_{12}$ and $A_2BV_3F_{12}$.

Considering that most Heisenberg-like KLAFs with some perturbations adopt 120° magnetic structures [31,33,35,38,39], it is most likely that $Cs_2KCr_3F_{12}$ and $Cs_2NaCr_3F_{12}$ also have 120° structures as the ground states. As mentioned before, 120° structures have chiral degrees of freedom in each triangle on the kagome lattice. The key to the ground states of $Cs_2BCr_3F_{12}$ is that both compounds only show in-plane spin canting, which is very rare in KLAFs such as $CdCu_3(OH)_6(NO_3)_2 \cdot H_2O$ [38], whereas out-of-plane spin canting was often reported in KLAFs [31,33,35,39]. In these compounds, the $q = 0$ 120° structures are realized in the kagome planes mainly due to the DM interaction $\boldsymbol{D}_{ij} \cdot S_i \times S_j$ [31,33,35,38]. The $q = 0$ 120° structures have two spin arrangements, a clockwise spin arrangement in all the triangles and a counterclockwise one, which depend on $\boldsymbol{D}_{ij}$ and are related to the direction of spin canting. Out-of-plane spin canting is stabilized for the $q = 0$ clockwise arrangement, while it is not for the counterclockwise one [22]. In contrast, as discussed by Okuma *et al.* [38], only the counterclockwise arrangement allows in-plane-spin canting. Thus, KLAFs $Cs_2BCr_3F_{12}$ with only in-plane canting are implied to have the $q = 0$ 120° structure with the counterclockwise arrangement. Moreover, relatively larger in-plane spin canting ($M_{sp}/S \sim 0.06\mu_B$/Cr) than that of $CdCu_3(OH)_6(NO_3)_2 \cdot H_2O$ [38] ($M_{sp}/S \sim 0.016\mu_B$/Cu) suggests that the small distortion of the kagome lattices in $Cs_2BCr_3F_{12}$, which produces several J_i in each Cr^{3+} triangle, also contributes to the in-plane spin canting [23,24].

As mentioned before, although in-plane spin canting occurs in each kagome layer of $Cs_2BCr_3F_{12}$, only $Cs_2KCr_3F_{12}$ shows M_{sp}, which suggests that the sign of the interlayer coupling differs between two compounds. Such a difference was also reported in jarosite $KFe_3(OH)_6(SO_4)_2$ [39,40] and $KCr_3(OH)_6(SO_4)_2$ [33]. In both compounds, the $q = 0$ 120° structure with the clockwise arrangement is realized as the ground states, and out-of-plane spin canting occurs in each layer mainly due to the DM interaction [33,39,40]. While $KCr_3(OH)_6(SO_4)_2$ has M_{sp} due to a ferromagnetic interlayer coupling [33], $KFe_3(OH)_6(SO_4)_2$ shows no M_{sp} due to an antiferromagnetic one [39,40]. Similarly, for $Cs_2NaCr_3F_{12}$, in-plane-canted moments are considered to be canceled out between the nearest-neighbor kagome planes due to a weak antiferromagnetic interlayer coupling J_{inter} ($\sim 0.5\mu_B T \ll k_B|\theta_{CW}|$). Although the interlayer-superexchange-interaction paths Cr-F-Cs (B)-F-Cr are complicated, a rapid change of the sliding of the kagome plane in $Cs_2KCr_3F_{12}$ at T_S would induce subtle changes of the interlayer-superexchange paths, which may cause a change in the sign of the interlayer coupling.

Until now, we have discussed the ground states of $Cs_2BCr_3F_{12}$ considering those of other kagome systems. To elucidate the effects of quantum fluctuation on the ground states, it is important to compare the crystal structures and the ground states of $Cs_2BCr_3F_{12}$ with those of KLAFs $S = 1/2$ $A_2BTi_3F_{12}$ and $S = 1$ $A_2BV_3F_{12}$. Here, we look at the ground states of $A_2BTi_3F_{12}$ and $A_2BV_3F_{12}$. Three $S = 1/2$ $A_2BTi_3F_{12}$ show no magnetic ordering, and the ground states depend strongly on the distortion of the kagome lattices [43]. In contrast, three $S = 1$ $A_2BV_3F_{12}$ exhibit magnetic ordering with a 120° structure, whose spin plane is perpendicular to the kagome plane [44]. Thus, the ground state clearly differs among the three $S = 1/2$–$3/2$ spin systems $A_2BM_3F_{12}$.

We think that possible origins of the differences among the ground states of $A_2BM_3F_{12}$ are the distortion of the kagome lattice, magnetic anisotropy, the DM interaction, and quantum

fluctuation. In terms of magnetic anisotropy, $S = 1$ $A_2BV_3F_{12}$ have large Ising-like anisotropy, which mainly causes the 120° structure perpendicular to the kagome plane. Then, what is the main origin of the difference between the ground states of $A_2BTi_3F_{12}$ and $Cs_2BCr_3F_{12}$. As mentioned before, the DM interaction [21] and the distortion [23,24] stabilize magnetic ordering. However, the distortion of $Cs_2BCr_3F_{12}$ is smaller than that of $A_2BTi_3F_{12}$ with each B, and in particular the distortion of $Cs_2KCr_3F_{12}$ is very small. Regarding the DM interaction, the magnitude is roughly proportional to that of the spin-orbit interaction $\lambda \boldsymbol{L} \cdot \boldsymbol{S}$ ($\lambda = 155$ cm^{-1} for Ti^{3+} [49] and $= 92$ cm^{-1} for Cr^{3+} [49]). Considering that Cr^{3+} with t_{2g}^3 electronic configuration has no residual orbital moment, the magnitude of the DM interaction of $Cs_2BCr_3F_{12}$ is considered to be smaller than that of $A_2BTi_3F_{12}$. Thus, the formation of an in-plane-120° structure in $Cs_2BCr_3F_{12}$ is mainly due to a decrease of the quantum fluctuation. Paradoxically, our study experimentally suggests that the interplay between quantum fluctuation of $S = 1/2$ and spin frustration destroys long-range magnetic ordering even in KLAFs with some DM interaction and the distortion.

Although the ground state differs among $S = 1/2$–$3/2$ $A_2BM_3F_{12}$, there is a common feature in the magnetic properties under high magnetic fields. In addition to $Cs_2BCr_3F_{12}$, $S = 1/2$ $A_2BTi_3F_{12}$ show 1/3-magnetization-plateaulike behavior irrespective of the direction of H [43], whereas $S = 1$ $A_2BV_3F_{12}$ with Ising-like anisotropy exhibit distinct 1/3- and 2/3-magnetization plateaus under out-of-plane fields [44]. Thus, although there is a difference in the strength of the magnetic anisotropy, the 1/3-magnetization-plateaulike behavior is revealed to appear in $S = 1/2$–$3/2$ $A_2BM_3F_{12}$ including $S = 3/2$ Heisenberg-like KLAFs $Cs_2BCr_3F_{12}$, which is consistent with recent theoretical studies [19]. When we compare the M-H curves of $Cs_2BCr_3F_{12}$ with those of $A_2BTi_3F_{12}$, the 1/3-magnetization-plateaulike behavior of $Cs_2BCr_3F_{12}$ is less distinct than that of $A_2BTi_3F_{12}$, which is considered to be due to a decrease of the quantum fluctuation. In addition, unlike in the case of $S = 1/2$ $A_2BTi_3F_{12}$, the 1/3-magnetization-plateaulike behavior at 4.2 K is more distinctly observed than that at 1.3 K. This fact suggests that in $Cs_2BCr_3F_{12}$, thermal fluctuation is also important for the appearance of the 1/3-magnetization plateau, as is observed in $S = 3/2$ $KCr_3(OH)_6(SO_4)_2$ [33] with the same S.

V. CONCLUSION

We discovered two $S = 3/2$ kagome lattice antiferromagnets $Cs_2KCr_3F_{12}$ and $Cs_2NaCr_3F_{12}$ and succeeded in growing their single crystals. We also clarified the crystal structures and magnetic properties. While $Cs_2NaCr_3F_{12}$ crystallizes in a monoclinic system of $P2_1/m$, $Cs_2KCr_3F_{12}$ crystallizes in a monoclinic system of $C2/n$ at room temperature and the structure changes to a trigonal system of $P3_121$ at 270 K. Both compounds form antiferromagnetic ordering with in-plane spin canting in each kagome plane below 6 K, whereas spontaneous magnetization is only observed in $Cs_2KCr_3F_{12}$. The difference is due to the difference between the signs of the weak interlayer couplings, which may be related to the structural transition of $Cs_2KCr_3F_{12}$. The in-plane 120° structures in $Cs_2BCr_3F_{12}$ are remarkably different from disordered ground states in $A_2BTi_3F_{12}$ and out-of-plane 120° structures in $A_2BV_3F_{12}$, which is mainly due to the differences in the strength of quantum fluctuation and the strength of magnetic anisotropy for the three systems. Although the ground state differs, the 1/3-magnetization-plateaulike behavior is a common feature among $S = 1/2$–$3/2$ $A_2BM_3F_{12}$.

ACKNOWLEDGMENTS

This work was supported by JSPS KAKENHI Grant No. 15J02000 and a Grant-in-Aid for Scientific Research (C) from the Japan Society for the Promotion of Science (Grant No. 24540345). The synchrotron radiation experiments at the Photon Factory were performed with the approval of the Photon Factory Program Advisory Committee (Proposals No. 2014S2-002 and No. 2017G111). The synchrotron radiation experiments at the BL02B1 of SPring-8 were performed with the approval of the Japan Synchrotron Radiation Research Institute (JASRI) (Proposal No. 2017A1081).

[1] A. P. Ramirez, Annu. Rev. Mater. Sci. **24**, 453 (1994).
[2] L. Balents, Nature (London) **464**, 199 (2010).
[3] N. Elstner and A. P. Young, Phys. Rev. B **50**, 6871 (1994).
[4] Ch. Waldtmann, H.-U. Everts, B. Bernu, C. Lhuillier, P. Sindzingre, P. Lecheminant, and L. Pierre, Eur. Phys. J. B **2**, 501 (1998).
[5] G. Misguich, D. Serban, and V. Pasquier, Phys. Rev. Lett. **89**, 137202 (2002).
[6] S. Yan, D. A. Huse, and S. R. White, Sci. **332**, 1173 (2011).
[7] Y. M. Lu, Y. Ran, and P. A. Lee, Phys. Rev. B **83**, 224413 (2011).
[8] S. Depenbrock, I. P. McCulloch, and U. Schollwöck, Phys. Rev. Lett. **109**, 067201 (2012).
[9] S. Ryu, O. I. Motrunich, J. Alicea, and M. P. A. Fisher, Phys. Rev. B **75**, 184406 (2007).
[10] Y. Ran, M. Hermele, P. A. Lee, and X. G. Wen, Phys. Rev. Lett. **98**, 117205 (2007).
[11] M. Hermele, Y. Ran, P. A. Lee, and X. G. Wen, Phys. Rev. B **77**, 224413 (2008).
[12] H. J. Liao, Z. Y. Xie, J. Chen, Z. Y. Liu, H. D. Xie, R. Z. Huang, B. Normand, and T. Xiang, Phys. Rev. Lett. **118**, 137202 (2017).
[13] K. Hida, J. Phys. Soc. Jpn. **69**, 4003 (2000).
[14] S. Nishimoto and M. Nakamura, Phys. Rev. B **92**, 140412 (2015).
[15] H. Asakawa and M. Suzuki, Physica A **198**, 210 (1993).
[16] H. J. Changlani and A. M. Läuchli, Phys. Rev. B **91**, 100407 (2015).
[17] K. Hida, J. Phys. Soc. Jpn. **70**, 3673 (2001).
[18] S. Nishimoto, N. Shibata, and C. Hotta, Nat. Commun. **4**, 2287 (2013).
[19] T. Picot, M. Ziegler, R. Orús, and D. Poilblanc, Phys. Rev. B **93**, 060407 (2016).

[20] F. Kolley, S. Depenbrock, I. P. McCulloch, U. Schollwöck, and V. Alba, Phys. Rev. B **91**, 104418 (2015).
[21] O. Cépas, C. M. Fong, P. W. Leung, and C. Lhuillier, Phys. Rev. B **78**, 140405 (2008).
[22] M. Elhajal, B. Canals, and C. Lacroix, Phys. Rev. B **66**, 014422 (2002).
[23] T. Yavors'kii, W. Apel, and H.-U. Everts, Phys. Rev. B **76**, 064430 (2007).
[24] P. H. Y. Li, R. F. Bishop, C. E. Campbell, D. J. J. Farnell, O. Götze, and J. Richter, Phys. Rev. B **86**, 214403 (2012).
[25] M. P. Shores, E. A. Nytko, B. M. Bartlett, and D. G. Nocera, J. Am. Chem. Soc. **127**, 13462 (2005).
[26] P. Mendels, F. Bert, M. A. de Vries, A. Olariu, A. Harrison, F. Duc, J. C. Trombe, J. S. Lord, A. Amato, and C. Baines, Phys. Rev. Lett. **98**, 077204 (2007).
[27] J. S. Helton, K. Matan, M. P. Shores, E. A. Nytko, B. M. Bartlett, Y. Yoshida, Y. Takano, A. Suslov, Y. Qiu, J.-H. Chung, D. G. Nocera, and Y. S. Lee, Phys. Rev. Lett. **98**, 107204 (2007).
[28] M. Fu, T. Imai, T.-H. Han, and Y. S. Lee, Science **350**, 655 (2015).
[29] T.-H. Han, M. R. Norman, J.-J. Wen, J. A. Rodriguez-Rivera, J. S. Helton, C. Broholm, and Y. S. Lee, Phys. Rev. B **94**, 060409 (2016).
[30] H. Yoshida, Y. Michiue, E. Takayama-Muromachi, and M. Isobe, J. Mater. Chem. **22**, 18793 (2012).
[31] M. Yoshida, Y. Okamoto, M. Takigawa, and Z. Hiroi, J. Phys. Soc. Jpn. **82**, 013702 (2013).
[32] J. A. Quilliam, F. Bert, R. H. Colman, D. Boldrin, A. S. Wills, and P. Mendels, Phys. Rev. B **84**, 180401 (2011).
[33] K. Okuta, S. Hara, H. Sato, Y. Narumi, and K. Kindo, J. Phys. Soc. Jpn. **80**, 063703 (2011).
[34] S. Okubo, R. Nakata, S. Ikeda, N. Takahashi, T. Sakurai, W.-M. Zhang, H. Ohta, T. Shimokawa, T. Sakai, K. Okuta, S. Hara, and H. Sato, J. Phys. Soc. Jpn. **86**, 024703 (2017).
[35] T. Ono, K. Morita, M. Yano, H. Tanaka, K. Fujii, H. Uekusa, Y. Narumi, and K. Kindo, Phys. Rev. B **79**, 174407 (2009).
[36] L. J. Downie, E. I. Ardashnikova, C. C. Tang, A. N. Vasiliev, P. S. Berdonosov, V. A. Dolgikh, M. A. de Vries, and P. Lightfoot, Crystals **5**, 226 (2015).
[37] E. A. Nytko, J. S. Helton, P. Müller, and D. G. Nocera, J. Am. Chem. Soc. **130**, 2922 (2008).
[38] R. Okuma, T. Yajima, D. Nishio-Hamane, T. Okubo, and Z. Hiroi, Phys. Rev. B **95**, 094427 (2017).
[39] T. Inami, M. Nishiyama, S. Maegawa, and Y. Oka, Phys. Rev. B **61**, 12181 (2000).
[40] M. Nishiyama, S. Maegawa, T. Inami, and Y. Oka, Phys. Rev. B **67**, 224435 (2003).
[41] N. Wada, T. Kobayashi, H. Yano, T. Okuno, A. Yamaguchi, and K. Awaga, J. Phys. Soc. Jpn. **66**, 961 (1997).
[42] U. Englich, C. Frommen, and W. Massa. J. Alloys Compd. **246**, 155 (1997).
[43] M. Goto, H. Ueda, C. Michioka, A. Matsuo, K. Kindo, and K. Yoshimura, Phys. Rev. B **94**, 104432 (2016).
[44] M. Goto, H. Ueda, C. Michioka, A. Matsuo, K. Kindo, K. Sugawara, S. Kobayashi, N. Katayama, H. Sawa, and K. Yoshimura, Phys. Rev. B **95**, 134436 (2017).
[45] K. Sugimoto, H. Ohsumi, S. Aoyagi, E. Nishibori, C. Moriyoshi, Y. Kuroiwa, H. Sawa, and M. Takata, in *10th International Conference on Radiation Instrumentation SRI 2009*, edited by R. Garrett, I. Gentle, K. Nugent, and S. Wilkins, AIP Conf. Proc. No. 1234 (AIP, New York, 2010), p.887.
[46] K. Sugawara, K. Sugimoto, T. Fujii, T. Higuchi, N. Katayama, Y. Okamoto, and H. Sawa, J. Phys. Soc. Jpn. **87**, 024601 (2018).
[47] G. M. Sheldrick, *SHELXL*-97, Program for Structure Refinement (University of Göttingen, Germany, 1997).
[48] D. Babel, Z. Anorg. Allg. Chem. **387**, 161 (1972).
[49] B. N. Figgis, *Introduction to Ligand Fields* (Interscience, New York, 1966).